

Received July 8, 2019, accepted July 18, 2019, date of publication July 30, 2019, date of current version August 14, 2019.

Digital Object Identifier 10.1109/ACCESS.2019.2932091

# Implementation of Mass-Independent Impedance Control for RFSEA Using a Linkage Arm

KYEONGMIN KIM AND YOUNG SAM LEE<sup>ID</sup>

Department of Electrical Engineering, Inha University, Incheon 22212, South Korea

Corresponding author: Young Sam Lee (lys@inha.ac.kr)

This work was supported by the National Research Foundation of Korea (NRF) through the Korean Government (MOE) under Grant 2017R1D1A1B03029578.

**ABSTRACT** When using the powered lower-limb prosthesis, it is important to obtain varying amputee's weight to prevent an excessive knee flexion in the early stance phase of finite state impedance control. This paper proposes a method for implementing an impedance controller that can operate independently of the varying load mass for reaction force sensing elastic actuator (RFSEA) with a linkage arm. The proposed controller estimates the load mass using recursive least square. We apply a Kalman filter and a disturbance observer to improve the accuracy of the measurement and the tracking performance of the force controller, respectively. The results of an experiment applying a lab-developed RFSEA system with a linkage arm validate the feasibility of this approach. It is also expected that the proposed system reduces the size and development costs of the prosthesis due to the advantages of using the RFSEA.

**INDEX TERMS** Mass estimation, series elastic actuator, adaptive filters, recursive least square, disturbance observer, force control, impedance control.

## I. INTRODUCTION

Compared to a traditional passive lower-limb prosthesis, recent powered knee prostheses enable the reproduction of a more natural locomotion and provide various functions such as walking, running, sitting, and stair climbing [1], [2]. Assuming that locomotion is periodic, many powered knee prostheses use an impedance controller [3]–[5]. To use the impedance controller, many of the parameters need to be selected by clinicians. However, some parameters may not be appropriate, and the entire process requires a large amount of time and energy because clinicians must manually adjust the number of parameters by observing the patient's motion. Hence, many control methods have been studied to solve this problem. The adaptive control system used in a previously developed magnetorheological prosthetic knee in [6] creates the appropriate parameters by storing the gait cycle and axial force applied to the prosthesis after the amputee has performed the prescribed gait step. The learning system proposed in [7] produces desired joint trajectories corresponding to the amputee's physical characteristics by tracking the invariant trajectories and estimates controller parameters by

solving a parameter estimation problem. The auto-tuning system proposed in [8] configures the controller parameters by using fuzzy logic and a cyber expert system that encodes the factual knowledge or skills of a human expert into a computer system through a database. Although they provide many advantages, prostheses using such solutions are difficult to commercialize. Because many sensors are applied and the length of the prosthesis is not taken into account, the development cost of the device is high and it cannot be used by people with shorter lower limbs.

The knee extension angle is directly related to the change in weight of the amputee during the stance phase, during which all of the amputee's weight must be supported by a single foot. The knee prosthesis should be able to cope with weight changes caused by various factors that occur while walking because the angle of the knee extension affects the ambulation balance and safety during all situations, including running or walking on stairs, ramps, or a flat surface. Therefore, this study aims at the development of a method for estimating the change in the load mass allowing the impedance controller to operate independently of such mass with a low development cost.

The main reasons for the increasing development costs of wearable robots such as a powered prosthesis or

The associate editor coordinating the review of this manuscript and approving it for publication was Haiquan Zhao.

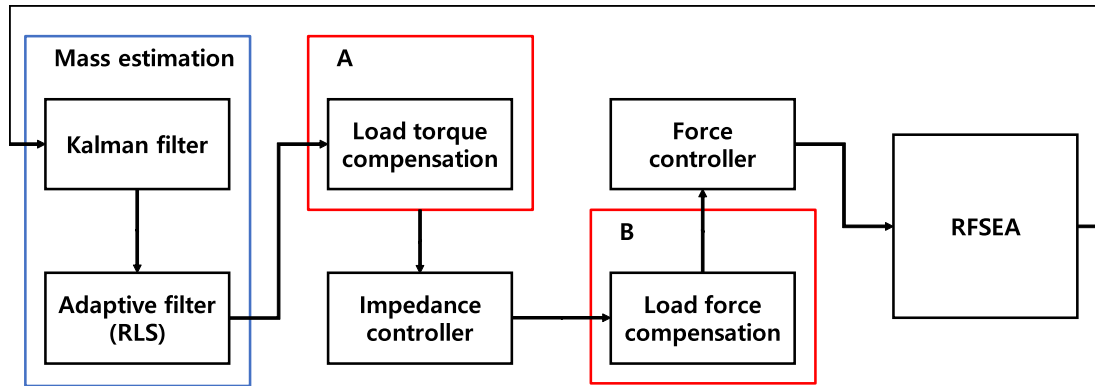


**FIGURE 1.** The proposed structure: Block A is the compensation block for the impedance controller. Block B is the compensation block for the force controller.

exoskeleton are the required robot joints and torque sensors (a strain-gauge or twist-angle type). Because a wearable robot is in direct contact with the user, despite the high cost, a torque sensor that can measure the external force applied from the environment, as well as the contact force, is essential to the user safety of a wearable robot [9]. Series elastic actuators (SEAs) and harmonic drive gears are the most commonly used devices in a robot joint. Unlike a harmonic drive gear, SEAs measure the force by using a spring like a torque sensor. The accuracy of the force controller is improved by interpreting the force control from the perspective of position control with respect to the spring length. In addition, SEAs act as low-pass filters and provide numerous advantages such as an increase in the peak force output and energy storage efficiency [10]. Owing to these advantages, SEAs are used in powered knee prostheses of different shapes and forms by configuring the type and structure of the compliant components according to the purposes of the user [11], [12]. Among the SEAs applying a screw, a reaction force sensing series elastic actuator (RFSEA) [13], [14] is one of the most compact structures available. The spring and motor are connected in parallel, reducing the size of RFSEA. In addition, because the spring is not required to move with the load and is placed behind the actuator, RFSEA has a more compact size and a significant range of motion for the travel length of the screw.

During the early stance of a walking motion, when the feet touch the ground, the sensor can measure the torque. Therefore, an estimation of the change in the user's weight should be achieved quickly. When the dynamics of the measurements are known, the recursive least squares (RLS) approach has appropriate properties for estimating the weight of the user wearing a powered knee prosthesis because the convergence speed of RLS is faster than other adaptive filters [15]–[17]. In this paper, we propose a method of implementation that allows the change in mass to be estimated using the RLS algorithm in RFSEA with a linkage arm and uses the estimated mass as the input to the force and impedance controllers such that the entire system operates independently of the mass. During this process, the acceleration required is

estimated using a Kalman filter to remove the time delay and noise. The estimated mass determined using RLS removes the torque generated by the load from the torque measured by the spring. As a result, the torque input into the impedance controller remains an independent element of the load mass, and the impedance controller can operate regardless of the load applied to the linkage arm when no external force is applied. The overall structure of the controller is shown in Fig. 1, which is described in greater detail in Section III. B.

The proposed method has the contributions that the powered knee prosthesis guarantees the appropriate knee flexion without adjusting the parameters during the stance phase by estimating the weight of the amputee, and the development costs can be reduced using only two encoders for the estimation. In addition, as an actuator of the prosthesis, RFSEA increases the versatility of the prosthesis for amputees with different leg lengths. The rest of the paper is organized as follows. Section II introduces the design of RFSEA. Section III describes the control approach. Section IV presents experimental results showing the estimated load mass and tracking performance. Finally, Section V provides some concluding remarks regarding this research.

## II. DESIGN OF REACTION FORCE SERIES ELASTIC ACTUATOR

There are many different types of SEAs depending on the structure of the actuators and the compliance required. The type of SEA built in our lab during this study is RFSEA proposed in [14]. As the main characteristic of RFSEA, when the motor torque is transmitted to the load, a spring can measure both this transmitted torque and the reaction torque. The motor used to power RFSEA is a Maxon EC-4 pole 200W BLDC motor. A pulley/ball screw reduction maximizes the mechanical power because it reduces any losses during transmission. The transmitted power rotates the ball nut and the screw moves in a straight line. The spring is placed around the ball screw support without adding to the length of the actuator. This structure increases the range of motion for the travel length of the ball screw and the compactness [14], [18].

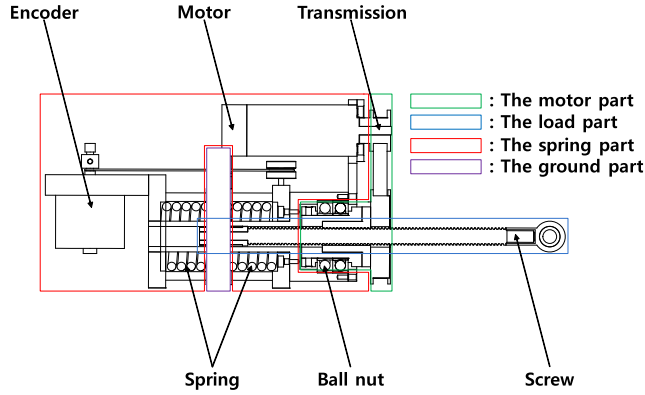


FIGURE 2. Structure of a lab-developed RFSEA.

The structure of RFSEA is shown in Fig. 2. The external and transmitted forces are measured using a spring with encoders. As the spring stiffness decreases, the energy storage increases along with the nonlinearity. Hence, the spring used is manufactured with a stiffness rate of 83.4 [N/mm] considering the peak force of the motor and the gear ratio. The stiffness of the entire spring is 166.8 [N/mm] because we use two springs installed using a pre-compression. The maximum force output is 897.2 [N]. Thus, we can measure a force of 5.38 [N] per 1 [mm] of spring deformation. A 5,000 count-per-revolution incremental encoder (E50S series rotary encoder manufactured by Autonics Company) is used to measure the force. We use this along with the interpolation method. As a result, the encoder has 20,000 counts per revolution.

### III. MODELING AND CONTROL

#### A. FORCE CONTROL

As the purpose of the force controller, the force measured by the spring is used to track the desired force. However, owing to the vibrations of the spring, the force controller of RFSEA cannot ensure fidelity at all frequencies. To solve this problem, the authors of [18] regulate the performance of the force controller at near the resonant frequencies. The structure of the force controller, constructed according to the method proposed in [18], is shown in Fig. 3. A PID controller compensates for unconsidered errors, but has a limitation in increasing the control gain. To improve the force

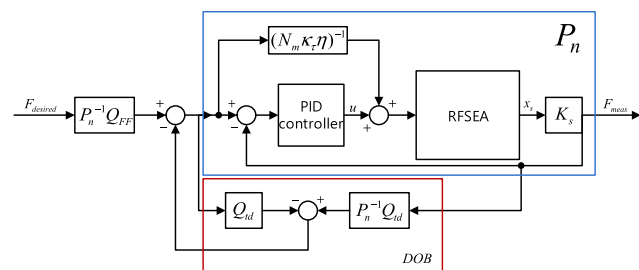


FIGURE 3. Block diagram of the force controller.

tracking performance and reduce the steady-state error, the disturbance observer (DOB) is used in the force controller. The DOB compensates for errors caused by the disturbance and incorrect plant modeling [19]. To use the DOB, the nominal function and a Q-filter are acquired.

The nominal plant transfer function is derived from the dynamics of RFSEA as follows:

$$\begin{aligned} M_s \ddot{x}_s + B_s \dot{x}_s + K_s x_s &= F_{trans}, \\ M_l \ddot{x}_l + B_l \dot{x}_l &= F_{trans} + F_{ext}, \\ J_m \ddot{\theta}_m + B_m \dot{\theta}_m &= \tau_m + N_m^{-1} F_{trans}. \end{aligned} \quad (1)$$

Here,  $M_s$  and  $M_l$  are the masses of the spring and load parts;  $J_m$  is the inertia of the motor part;  $B_s$ ,  $B_l$ , and  $B_m$  are the damping coefficients of the spring part, load part, and motor parts in the order given, respectively;  $K_s$  is the spring stiffness stated in section II;  $x_s$  is the position of the spring;  $F_{trans}$  is the force generated by the spring deformation,  $F_{ext}$  is the external force, and  $\tau_m$  is the force generated by the motor; and  $\theta_m$  is the motor angle. The values of  $x_s$  and  $\theta_m$  are measured by the encoder, and  $x_l$ , which is the position of the load, can be calculated through the following equation.

$$x_l = x_s + N_m^{-1} \theta_m, \quad (2)$$

where  $N_m$  is the speed reduction ratio, which defines the relationship between the actuator force ( $F_l$ ) and the motor torque ( $\tau_m$ ) as follows:

$$N_m = \frac{F_l}{\tau_m} = \frac{2\pi N_{pulley} \eta}{l_{lead}}. \quad (3)$$

$N_{pulley}$  is a pulley reduction, and  $\eta$  and  $l_{lead}$  are the drive train efficiency and ball screw lead, respectively. The steady-space equation of RFSEA is derived using (1) and (2) as follows:

$$\begin{aligned} \dot{x} &= Ax + Bu, \\ y &= Cx + Du, \end{aligned} \quad (4)$$

where

$$\begin{aligned} x &= [x_s \quad \dot{x}_s \quad x_l \quad \dot{x}_l]^T \\ u &= [\tau_m \quad F_{ext}]^T, \\ y &= [x_s \quad x_l]^T. \end{aligned} \quad (5)$$

In (4),  $A$ ,  $B$ ,  $C$ ,  $D$  are as follows:

$$\begin{aligned} A &= \begin{bmatrix} 0 & 1 & 0 & 0 \\ \frac{N_m^2 J_m K_s - M_l K_s}{a_1 N_m^2 J_m M_l} & \frac{B_s - a_3 M_l}{a_1 M_l} & 0 & \frac{M_l B_m - J_m B_l}{a_1 J_m M_l} \\ 0 & 0 & 0 & 1 \\ \frac{a_0 N_m^2 J_m K_s - M_s K_s}{a_0 a_2 N_m^2 J_m M_s} & \frac{a_0 B_s - a_3 M_s}{a_0 a_2 M_s} & 0 & \frac{M_s B_m - a_0 J_m B_l}{a_0 a_2 J_m M_s} \end{bmatrix}, \\ B &= \begin{bmatrix} 0 & 0 \\ \frac{1}{a_1 N_m J_m} & \frac{1}{a_1 M_l} \\ 0 & 0 \\ \frac{1}{a_0 a_2 N_m J_m} & \frac{1}{a_2 M_s} \end{bmatrix}, \end{aligned}$$

$$C = \begin{bmatrix} 0 & 1 & 0 & 0 \\ 0 & 0 & 1 & 0 \end{bmatrix},$$

$$D = \begin{bmatrix} 0 & 0 \\ 0 & 0 \end{bmatrix}, \quad (6)$$

where

$$a_0 = 1 + \frac{M_s}{N_m^2 J_m},$$

$$a_1 = 1 + \frac{M_s}{N_m^2 J_m} - \frac{M_s}{M_l},$$

$$a_2 = \frac{a_0 M_l - M_s}{a_0 M_s},$$

$$a_3 = \frac{N_m^2 B_m + B_s}{N_m^2 J_m}. \quad (7)$$

The parameters in (7) are obtained using the parameter optimization stated in [20], and are shown in Table 1.

TABLE 1. Estimated system parameters.

Parameter	Value
$J_m$	0.62e-05 [kg · m <sup>2</sup> ]
$B_m$	2.14e-04 [Nm · s/rad]
$M_l$	0/2.5/5.0/7.5 [kg]
$B_l$	170 [N · s/m]
$M_s$	1.6 [kg]
$B_s$	200 [N · s/m]
$K_s$	166712 [N/m]
$N_m$	9425

The nominal plant model for the DOB can be expressed using (4) as follows:

$$P_n(s) = \frac{F_{meas}}{F_{desired}} = \frac{K_n}{M_n s^2 + B_n s + K_n}, \quad (8)$$

where

$$M_n = \frac{N_m^2 J_m + M_s}{N_m k_\tau \rho + \eta^{-1}},$$

$$B_n = \frac{N_m^2 B_m + B_s}{N_m k_\tau \rho + \eta^{-1}},$$

$$K_n = K_s. \quad (9)$$

The measured output force is the input to the inverse of  $P_n$ . A Q filter is required to make the inverse plant model  $P_n$  realizable and to behave like a low-pass filter. Hence, the Q filter is expressed as a second-order Butterworth filter considering the degree of the plant model as follows:

$$Q(s) = \frac{1}{(s/w_c)^2 + 1.4142(s/w_c) + 1}, \quad (10)$$

where the cutoff frequency  $w_c$  is determined empirically. For more detailed information on the force controller and a discussion on the controller stability, refer to [14], [18]

Fig. 4 shows the results of the force tracking experiments. The desired force is 5 [N]. When using only a P controller with a feedforward filter, the result is biased against a desired force of approximately 0.8 [N]. However, when using the DOB with the previous controller, the output force of the load

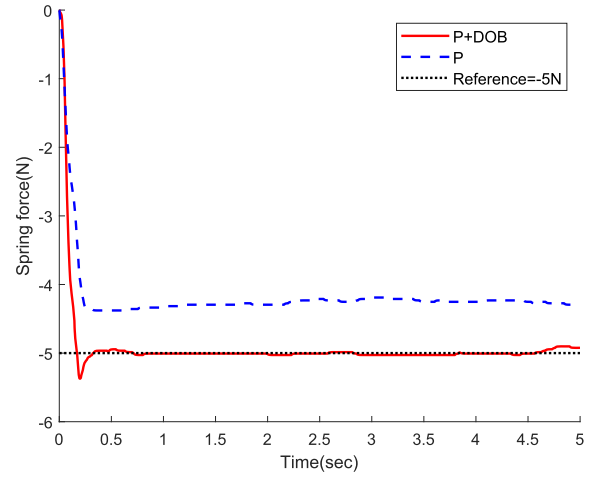


FIGURE 4. Comparative experimental results of the force controller: the P controller alone and the P+DOB controller.

follows the desired force due to compensation for the limited gain of the P controller by the DOB.

### B. IMPEDANCE CONTROL

In [21], the author proposes a concept in which the torque needed by each joint can be separately defined through a sequence of the passive impedance function for a single step cycle. Furthermore, in [22], the impedance model is defined using a function presented through a joint angle and its velocity. The impedance controller increases the stability of the contact surface between the user and the actuator because it can respond to both the contact force and the externally applied force [23]. Due to these features, the finite-state impedance control is most widely used to control the powered knee prosthesis.

The simplified impedance model used in this paper is defined as follows:

$$\tau = B_d (\dot{\theta}_d - \dot{\theta}_r) + K_d (\theta_d - \theta_r),$$

$$= B_d \Delta \dot{\theta} + K_d \Delta \theta. \quad (11)$$

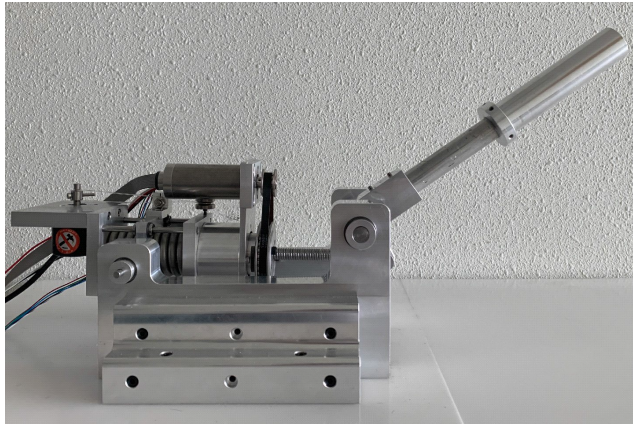
where  $\tau$  is the contact torque,  $B_d$  and  $K_d$  are the desired damping coefficient and spring stiffness, respectively;  $\theta_d$  is the desired joint angle; and  $\theta_r$  is the joint angle. In general, the impedance model uses the contact torque and joint angle to create the desired joint angle through the method proposed in [24]. The desired joint angle can be easily obtained using the following equation.

$$\theta_d = \theta_r + \Delta \theta, \quad (12)$$

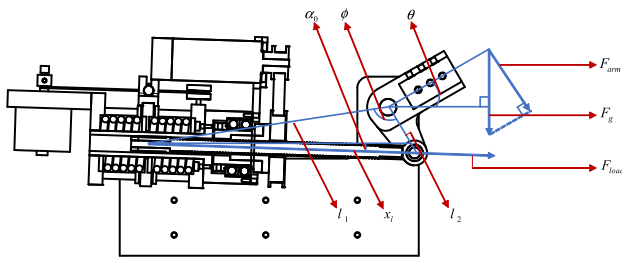
where

$$\Delta \theta = h(\tau) = \frac{\tau}{B_d s + K_d}. \quad (13)$$

However, a problem exists in that, if the characteristics of the user are changed after the parameter has been selected by the clinician, the impedance model might operate abnormally. In particular, during the stance phase, the damping coefficient



(a) Laboratory-built RFSEA system.



(b) The structure of RFSEA with linkage arm.

FIGURE 5. RFSEA with a linkage arm.

is adjusted such that the knee can bend at an appropriate angle in consideration of the user's weight. To solve this problem, we estimate and compensate the load weight for the input torque into the impedance model and a force controller to operate the impedance controller independent of the load mass.

For the experiment on the mass estimation and to clarify the desired angle tracking result, RFSEA is constructed as shown in Fig. 5. Fig. 5 (b) also shows the direction of the actuator force ( $F_{load}$ ), the force ( $F_g$ ) of the load mass from gravity, the angle, and the lengths of each part. Based on the principles of a virtual operation, the arm torque generated by the actuator force depends on the arm angle ( $\theta$ ) using the following equation.

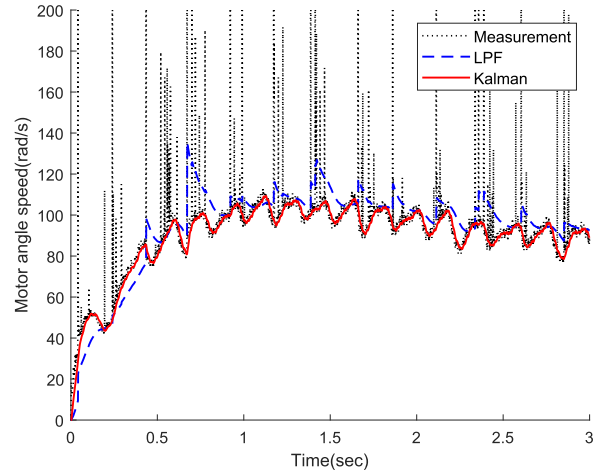
$$\tau_L = \frac{\partial x_l}{\partial \phi} F_l = f(\phi) F_l, \quad (14)$$

where  $f(\phi)$  is

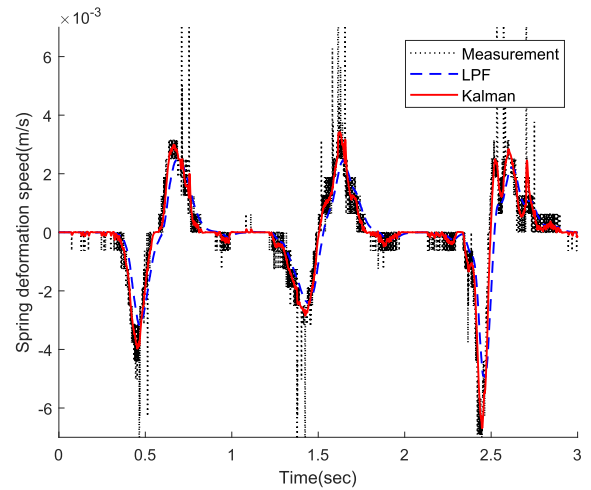
$$f(\phi) = \frac{l_1 + l_2 + \sin \phi}{\sqrt{l_1^2 + l_2^2 - 2l_1 l_2 \cos \phi}}. \quad (15)$$

The dynamics of a linkage arm indicate the relation between the arm torque and arm angle with the arm inertia  $J$  as follows:

$$\tau_L = J_a \ddot{\theta} - \tau_g. \quad (16)$$



(a) Estimated acceleration of the motor angle.



(b) Estimated acceleration of the spring deformation.

FIGURE 6. Comparative experimental results of filtering: Using the low-pass filter, using the Kalman filter, and measurement.

In (16),  $\tau_g$  is defined as

$$\tau_g = g(m, \theta) = r F_{arm} = r F_g \cos \theta = r m g \cos \theta, \quad (17)$$

where  $F_{arm}$  is orthogonal to the linkage arm. Combining (16) and (17), we obtain the following equation relating the arm torque to the arm angle and the torque from gravity:

$$\tau_L = J_a \ddot{\theta} - r m g \cos \theta. \quad (18)$$

The arm angle can be calculated as

$$\theta = \arccos \left( \frac{l_1^2 + l_2^2 - x_l^2}{2l_1 l_2} \right) + \alpha_0 - \frac{\phi}{2}. \quad (19)$$

where  $\alpha_0$  is the correction angle shown in Fig. 5 (b) and  $x_l$  is obtained through (19). Because all components except  $x_l$  are constant, the noise that occurs when calculating the angular acceleration of the arm angle is caused by  $x_l$  owing to the quantization noise of the encoder. Because  $x_s$  and  $\theta_m$ , which are used to obtain  $x_l$ , are measured by the encoder, we can

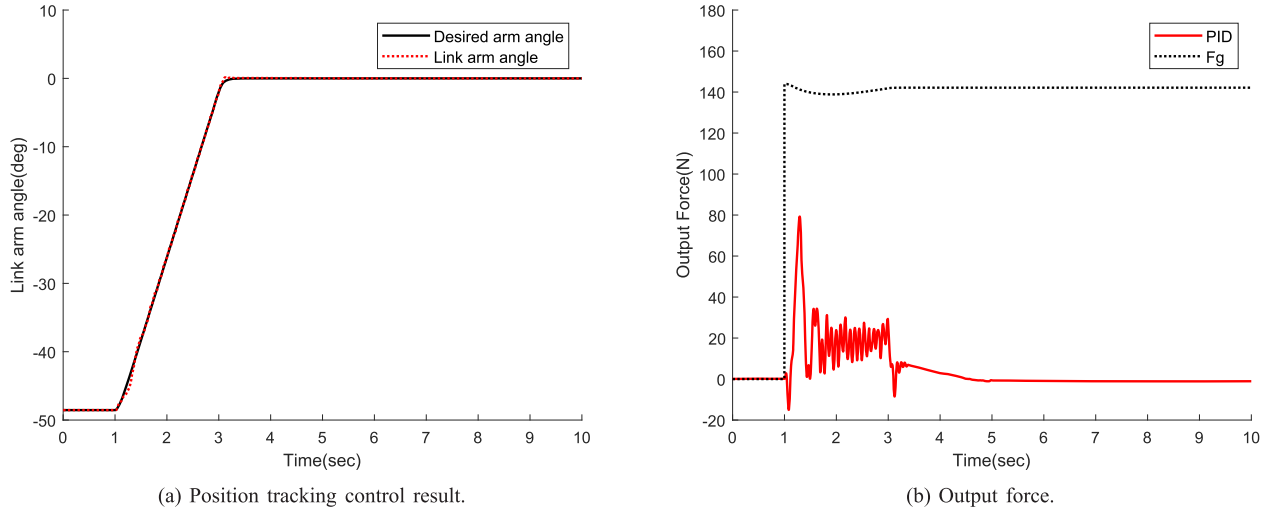


FIGURE 7. Experimental results of torque compensation for the force controller.

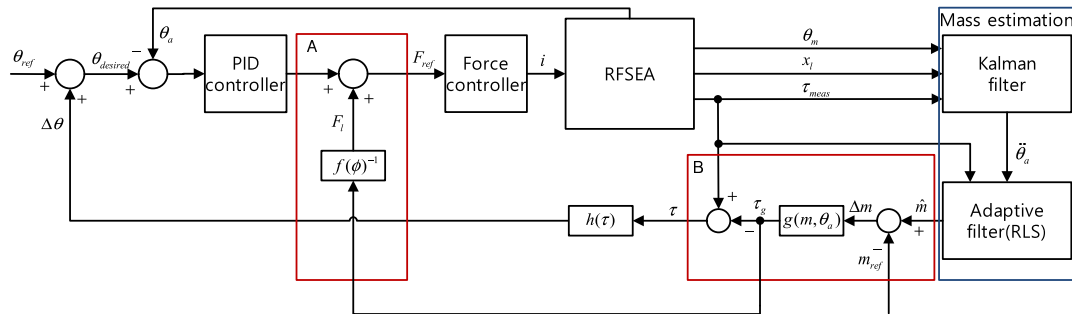


FIGURE 8. Detailed block diagram of torque compensation part of the impedance controller.

use a low-pass filter to attenuate the noise, causing a time-delay. Hence, by employing a Kalman filter, we can obtain the angular velocity of the arm without noise or a time delay. The following dynamic equation used in the Kalman filter is derived from (1).

$$\begin{aligned}
 x_{1,n+1} &= \begin{bmatrix} \theta_{m,n} + \dot{\theta}_{m,n} \Delta t \\ \dot{\theta}_{m,n} + \Omega_1 \Delta t \end{bmatrix}, \\
 x_{2,n+1} &= \begin{bmatrix} x_{s,n} + \dot{x}_{s,n} \Delta t \\ \dot{x}_{s,n} + \Omega_2 \Delta t \end{bmatrix}, \quad (20)
 \end{aligned}$$

where

$$\begin{aligned}
 \Omega_1 &= -\left(\frac{B_m}{J_m} - \frac{1}{J_m} \tau_{m,n} - \frac{N_m^{-1}}{J_m} F_{trans,n}\right), \\
 \Omega_2 &= -\left(\frac{B_s}{M_s} \dot{x}_{s,n}^{-1} + \frac{K_s}{M_s} x_{s,n} - \frac{1}{M_s} F_{trans,n}\right). \quad (21)
 \end{aligned}$$

Thus, we can derive the following discrete models when considering the process ( $w$ ) and measurement ( $v$ ) noises.

$$\begin{aligned}
 x_{1,n+1} &= A_1 x_{1,n} + w_{1,n}, \\
 y_{1,n} &= C_1 x_{1,n} + v_{1,n}, \\
 x_{2,n+1} &= A_2 x_{2,n} + w_{2,n}, \\
 y_{2,n} &= C_2 x_{2,n} + v_{2,n}. \quad (22)
 \end{aligned}$$

Using (22), the Kalman filter is designed according to [25]. The estimated results are shown in Fig. 6. The use of a low-pass filter can reduce noise from the angular speed of the motor and the speed of the spring deformation, although a time delay is incurred.

$$m = (g r \cos \theta)^{-1} (J_a \ddot{\theta} - \tau_L). \quad (23)$$

However, the estimated values when using a Kalman filter can be achieved without noise or a time delay. In addition,  $\ddot{\theta}$  can be obtained by further differentiating  $\theta_m$  and  $x_s$ .

The load mass can be acquired using the following equation with (18).

However, when measuring  $\tau_L$ , measurement noise results in inaccuracies of the mass estimation. To obtain better results, an adaptive filter is used to estimate the load mass.

In general, the prosthesis can measure the torque when its foot touches the ground. The convergence rate of RLS is faster than that of other adaptive filters such as a least squares estimation or a normalized least squares estimation because RLS finds the optimal solution to minimize the cost function at each sampling time [15], [16]. Therefore, RLS is suitable to achieve an estimation within a short amount of time.

The cost function of RLS is as follows:

$$J = \frac{1}{2} \sum_{i=1}^k \lambda^{k-i} e_i^2, \quad (24)$$

where  $e_i$  is the error between the measurement and estimated values, and  $\lambda$  is the forgetting factor. The exponential forgetting factor  $\lambda$  ( $0 < \lambda \leq 1$ ) controls the performance, including the tracking, improper adjustments, and ability since it weighs new data more heavily than old data [26].  $e_i$  is expressed as follows:

$$e_i = \tau_{L,i} - \sigma^T \hat{\theta}_i, \quad (25)$$

where  $\sigma$  and  $\hat{\theta}$  are

$$\begin{aligned} \sigma &= [\ddot{\theta} \quad -gr \cos \theta]^T, \\ \hat{\theta} &= [J_a \quad \hat{m}]^T. \end{aligned} \quad (26)$$

$\hat{m}$  is the estimated load mass and  $J_a$  is the inertia of the arm. To minimize the cost function  $J$ , a solution to the following equation should be found.

$$\frac{\partial J}{\partial \hat{\theta}} = 0. \quad (27)$$

The solution  $\hat{\theta}$  of (27) is calculated by following a recursive form.

$$\hat{\theta}_k = \hat{\theta}_{k-1} + K_k(\tau_{L,k} - \sigma_k^T \hat{\theta}_{k-1}), \quad (28)$$

where  $K_k$  is the gain as follows:

$$K_k = \frac{\lambda^{-1} P_{k-1} \sigma_k}{1 + \lambda^{-1} \sigma_k^T P_{k-1} \sigma_k}. \quad (29)$$

$P_k$  is the inverse correlation matrix as follows:

$$P_k = \lambda^{-1} P_{k-1} - \lambda^{-1} K_k \sigma_k^T P_{k-1}. \quad (30)$$

The estimated load mass is used to compensate for the torque generated by the load. Combining (14) and (17), the force generated by the screw to maintain the linkage arm at  $\theta_{desired}$  is

$$F_l = f(\phi)^{-1} \tau_g = f(\phi)^{-1} r F_g \cos \theta_a. \quad (31)$$

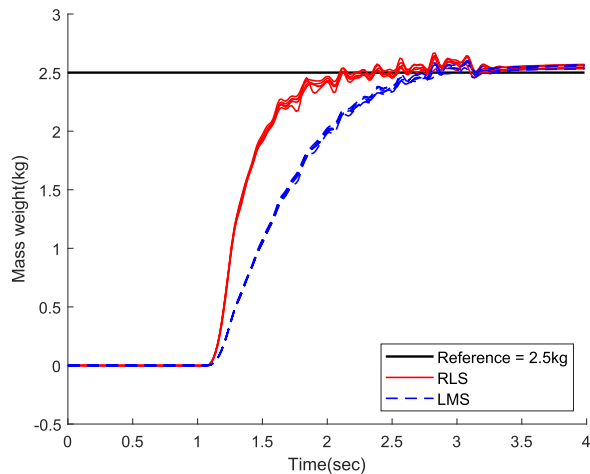
The torque input into the impedance model used to operate the impedance controller regardless of the change in the load mass is as follows.

$$\tau = \tau_{meas} - g(\Delta m, \theta a), \quad (32)$$

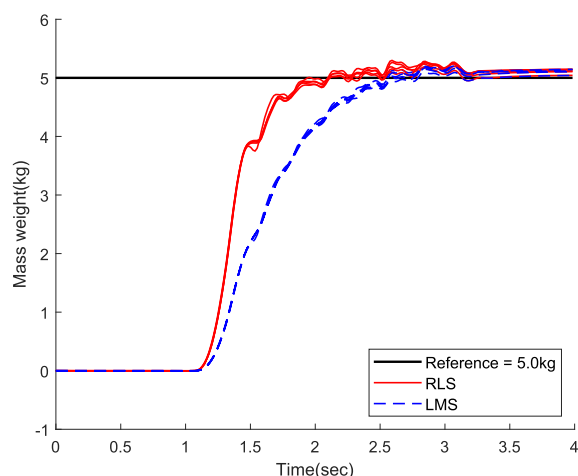
where  $m$  is calculated by the following equation.

$$\Delta m = \hat{m} - m_{ref}. \quad (33)$$

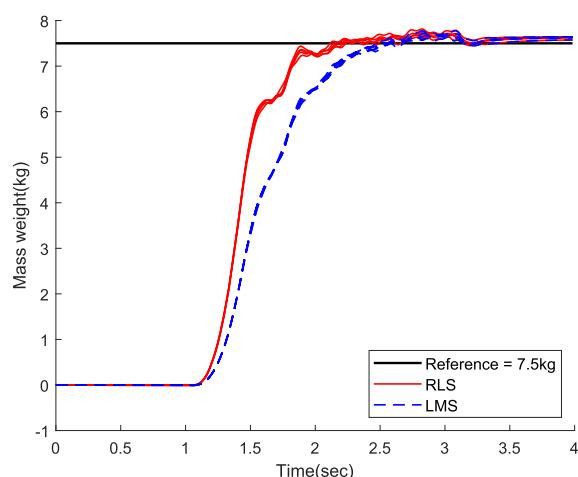
The PID controller can operate independently of the load mass by continuously compensating  $F_l$  for the force controller. This results in an increase in efficiency by eliminating the process of readjusting the PID parameters according to change in the load mass. Fig. 7 shows the position tracking



(a) 2.5kg.



(b) 5.0kg.



(c) 7.5kg.

FIGURE 9. The initial load mass estimation: LMS, RLS, and the actual load mass (reference).

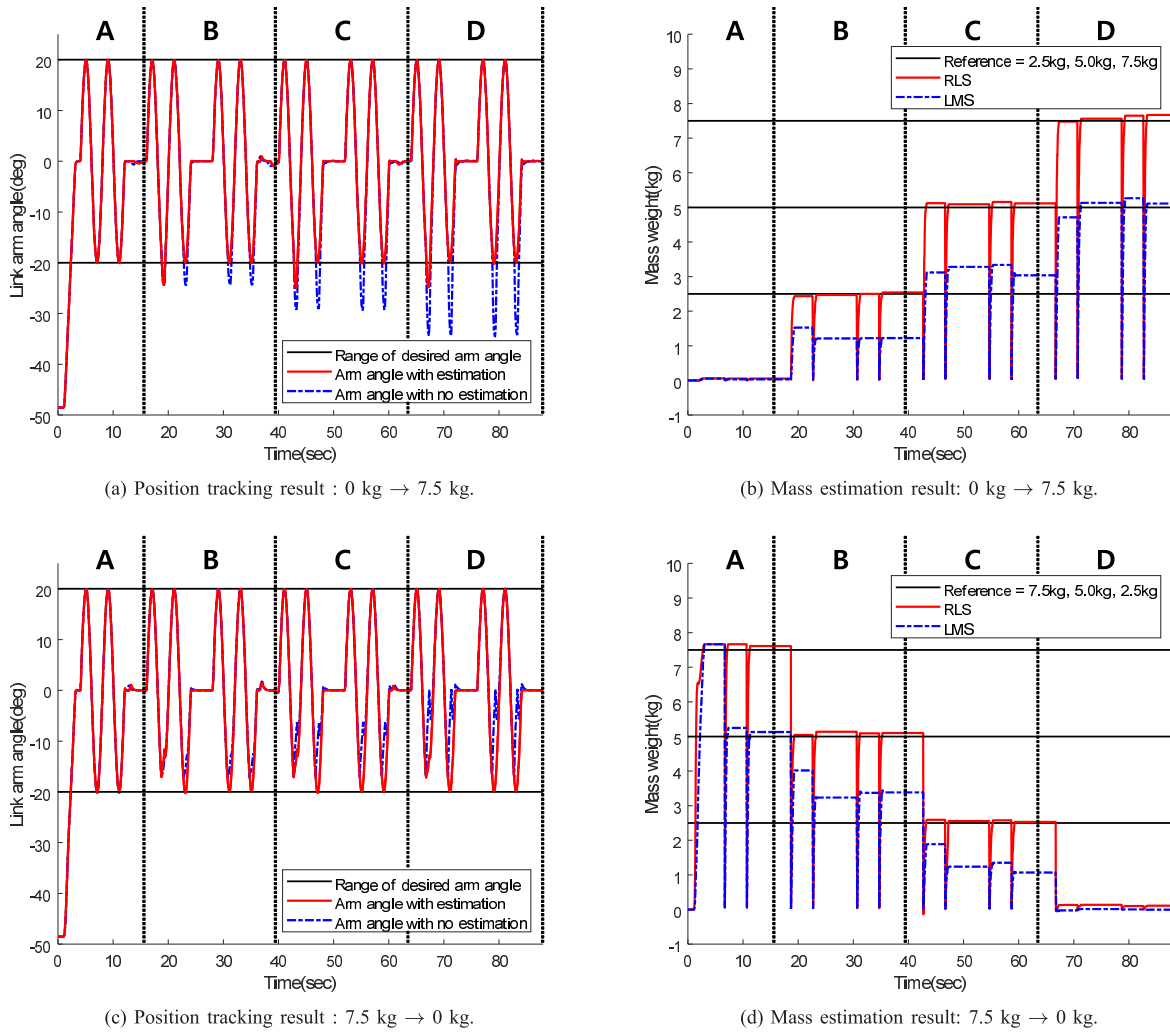


**FIGURE 10.** Experimental results of the impedance controller with the load mass estimation: In position tracking result, impedance controller, impedance controller with estimation, and the range of desired arm angle. In mass estimation result, LMS, RLS, and the actual load mass (reference).

result and outputs of the PID controller and the feedforward term ( $F_f$ ). As shown in Fig. 7 (b), after 3 seconds, most of the torque used to maintain the linkage arm at the desired angle is compensated by the output of the feedforward term.

Fig. 8 shows the specific structure of the impedance controller with the compensation parts previously shown in Fig. 1. In block A of Fig. 8,  $\tau_e$  is converted into  $F_f$  by (15), and  $F_f$  is added to the output of the PID controller. In block B of Fig. 8,  $\tau$  is used as the input to the impedance model using (17) and (32).

**IV. EXPERIMENT**

In this paper, the experiment was conducted by applying a disc-type load to the lab-built RFSEA with a linkage arm. The experiment was designed to identify the possibility of the powered knee prosthesis estimating the user’s weight while the prosthetic foot touches the ground. Therefore, RFSEA can only measure the torque for approximately 0.3 seconds

before and after the lowest points of the desired sinusoidal angle.

Initially, a linkage arm moves from the initial angle to the reference angle ( $0^\circ$ ) for 3 seconds, where the initial load mass is estimated. After this process, to change the load mass, the desired angle stops for one cycle after two cycles have been applied.

The results of the estimated initial load mass during the first 3 seconds are shown in Fig. 9. When the linkage arm reaches the reference angle, both filters converge at the same value. However, at 1.5 seconds, the error rates of the actual and estimated load masses of LMS and RLS are 57.77% and 25.57%, respectively, and are 17.18% and 2.444% at 2.0 seconds. These results imply that when LMS is used for the estimation, the estimated load mass converges more slowly near the actual load mass when compared to the use of RLS. In this case, the difference between the actual and estimated load masses is due to the unconsidered structure of RFSEA.

Fig. 10 shows the results of the path tracking through the impedance controller when the torque input to the impedance model changes owing to the varying load mass occurring from a linkage arm in motion. The impedance model can generate the angle added to the reference angle  $\theta_{ref}$  shown in Fig. 8 when torque is measured near the lowest point of the desired sinusoidal angle. If the estimated load mass is equal to the actual load mass, there will be no angle added to the desired sinusoidal angle because the target impedance model is set up to avoid generating any angle under a no-load condition.

Fig. 10 (a) and (b) show the results obtained when the load mass increasingly changes. Sections A, B, C, and D indicate 0.0, 2.5, 5.0, and 7.5 kg, respectively. In Fig. 10 (a), the dash-dotted line shows the results when no estimation is made. The lowest point of the path becomes even lower because the torque input into the impedance model increases as the load mass is added. However, when applying an estimation, a linkage arm moves along the same desired path because the angle added to the reference path is almost zero. At this time, the lowest point of the path is lowered at the first cycle in each section after changing the load mass because it uses the previously estimated information. Fig. 10 (b) shows the results of the estimation from near the lowest point. For the first 3 seconds, the RLS and LMS approaches converge at the same value because sufficient time is available. However, at near the lowest point, the results show that the load mass estimated by LMS, whose convergence speed is slower than RLS, does not reach the actual load mass. The load mass estimation error rates of RLS and LMS are 1.726% and 38.97%, respectively. The use of RLS is, therefore, 23-times more accurate than the use of LMS. Fig. 10 (c) and (d) shows the results obtained when the load mass decreases. Sections, B, C, and D indicate 7.5, 5.0, 2.5, and 0.0 kg, respectively. The results are the same as before, except that the lowest point becomes higher when the load mass is reduced. The error rates of the load mass estimation are 2.134% for RLS and 35.45% for LMS. The use of RLS is thus 17-times more accurate than the use of LMS.

## V. CONCLUSION

In this paper, we proposed a method applied to a lab-developed RFSEA system that prevents a change in the dynamic behavior of the impedance model set based on the initial load through a mass estimation when the load mass changes. The experimental results show that the proposed controller can track the desired path while maintaining the initially desired impedance performance regardless of the load mass variation without readjustment of the parameters. In this process, it was illustrated that RLS is more accurate than LSE when estimating the load mass within a short period of time. The proposed system is expected to contribute to the stability enhancement by preventing excessive knee flexion. It is also expected that the size and development costs by using RFSEA in the powered knee prosthesis.

## REFERENCES

- [1] F. Sup, H. A. Varol, and M. Goldfarb, "Upslope walking with a powered knee and ankle prosthesis: Initial results with an amputee subject," *IEEE Trans. Neural Syst. Rehabil. Eng.*, vol. 19, no. 1, pp. 71–78, Feb. 2011.
- [2] H. A. Varol, F. Sup, and M. Goldfarb, "Multiclass real-time intent recognition of a powered lower limb prosthesis," *IEEE Trans. Biomed. Eng.*, vol. 57, no. 3, pp. 542–551, Mar. 2010.
- [3] F. Sup, A. Bohara, and M. Goldfarb, "Design and control of a powered knee and ankle prosthesis," in *Proc. IEEE Int. Conf. Robot. Autom.*, Apr. 2007, pp. 4134–4139.
- [4] K. Fite, J. Mitchell, F. Sup, and M. Goldfarb, "Design and control of an electrically powered knee prosthesis," in *Proc. IEEE 10th Int. Conf. Rehabil. Robot.*, Jun. 2007, pp. 902–905.
- [5] F. Sup, A. Bohara, and M. Goldfarb, "Design and control of a powered transfemoral prosthesis," *Int. J. Robot. Res.*, vol. 27, no. 2, pp. 263–273, 2008.
- [6] H. Herr and A. Wilkenfeld, "User-adaptive control of a magnetorheological prosthetic knee," *Ind. Robot.*, vol. 30, no. 1, pp. 42–55, 2003.
- [7] N. Aghasadeghi, H. Zhao, L. J. Hargrove, A. D. Ames, E. J. Perreault, and T. Bretl, "Learning impedance controller parameters for lower-limb prostheses," in *Proc. IEEE/RSJ Int. Conf. Intell. Robots Syst.*, Nov. 2013, pp. 4268–4274.
- [8] H. Huang, D. L. Crouch, M. Liu, G. S. Sawicki, and D. Wang, "A cyber expert system for auto-tuning powered prosthesis impedance control parameters," *Ann. Biomed. Eng.*, vol. 44, no. 5, pp. 1613–1624, 2016.
- [9] D. E. Whitney, "Historical perspective and state of the art in robot force control," *Int. J. Robot. Res.*, vol. 6, no. 1, pp. 3–14, 1987.
- [10] G. A. Pratt and M. M. Williamson, "Series elastic actuators," in *Proc. IEEE/RSJ Int. Conf. Intell. Robots Syst.*, vol. 1, Aug. 1995, pp. 399–406.
- [11] E. C. Martinez-Villalpando, L. Mooney, G. Elliott, and H. Herr, "Antagonistic active knee prosthesis. A metabolic cost of walking comparison with a variable-damping prosthetic knee," in *Proc. Annu. Int. Conf. IEEE Eng. Med. Biol. Soc.*, Aug./Sep. 2011, pp. 8519–8522.
- [12] E. J. Rouse, L. M. Mooney, and H. M. Herr, "Clutchable series-elastic actuator: Implications for prosthetic knee design," *Int. J. Robot. Res.*, vol. 33, no. 13, pp. 1611–1625, 2014.
- [13] J. Pratt, B. Krupp, and C. Morse, "Series elastic actuators for high fidelity force control," *Ind. Robot, Int. J.*, vol. 29, no. 3, pp. 234–241, 2002.
- [14] N. Paine and L. Sentis, "A new prismatic series elastic actuator with compact size and high performance," in *Proc. IEEE Int. Conf. Robot. Biomimetics (ROBIO)*, Dec. 2012, pp. 1759–1766.
- [15] S. M. Kay, *Fundamentals of Statistical Signal Processing*. Upper Saddle River, NJ, USA: Prentice-Hall, 1993.
- [16] S. S. Haykin, *Adaptive Filter Theory*. New Delhi, India: Pearson Education, 2005.
- [17] J. Dhiman, S. Ahmad, and K. Gulia, "Comparison between adaptive filter algorithms (LMS, NLMS AND RLS)," *Int. J. Sci., Eng. Technol. Res.*, vol. 2, no. 5, pp. 1100–1103, 2013.
- [18] N. Paine, S. Oh, and L. Sentis, "Design and control considerations for high-performance series elastic actuators," *IEEE/ASME Trans. Mechatronics*, vol. 19, no. 3, pp. 1080–1091, Jun. 2014.
- [19] W.-H. Chen, J. Yang, L. Guo, and S. Li, "Disturbance-observer-based control and related methods—An overview," *IEEE Trans. Ind. Electron.*, vol. 63, no. 2, pp. 1083–1095, Feb. 2016.
- [20] K. Graichen, M. Treuer, and M. Zeitz, "Swing-up of the double pendulum on a cart by feedforward and feedback control with experimental validation," *Automatica*, vol. 43, no. 1, pp. 63–71, Jan. 2007.
- [21] N. Hogan, "Impedance control: An approach to manipulation," in *Proc. Amer. Control Conf.*, Jun. 1984, pp. 304–313.
- [22] D. A. Winter, *The Biomechanics and Motor Control of Human Gait: Normal, Elderly and Pathological*, 2nd ed. Ontario, FL, Canada: Univ. Waterloo Press, 1991.
- [23] T. Valency and M. Zacksenhouse, "Instantaneous model impedance control for robots," in *Proc. IEEE/RSJ Int. Conf. Intell. Robots Syst. (IROS)*, vol. 1, Oct./Nov. 2000, pp. 757–762.
- [24] D. A. Lawrence, "Impedance control stability properties in common implementations," in *Proc. IEEE Int. Conf. Robot. Autom.*, Apr. 1988, pp. 1185–1190.
- [25] M. S. Grewal and A. P. Andrews, *Kalman Filtering: Theory and Practice Using MATLAB*, 3rd ed. Hoboken, NJ, USA: Wiley, 2008.
- [26] S. Ciochina, C. Paleologu, J. Benesty, and A. A. Enescu, "On the influence of the forgetting factor of the RLS adaptive filter in system identification," in *Proc. Int. Symp. Signals, Circuits Syst.*, Jul. 2009, pp. 1–4.



**KYEONGMIN KIM** received the B.S. degree in electrical engineering from Inha University, Incheon, South Korea, in 2018, where he is currently pursuing the M.S. degree in electrical engineering. His research interests include design and control of actuators and system for dynamic legged robot, assistive devices for people, and embedded systems.



**YOUNG SAM LEE** received the B.S. and M.S. degrees from Inha University, Incheon, South Korea, in 1999, and the Ph.D. degree from Seoul National University, South Korea, in 2003, all in electrical engineering. From 2003 to 2004, he was a Senior Researcher with Samsung Electronics Company. Since 2004, he has been with the Department of Electrical Engineering, Inha University, Incheon. He has authored more than 50 articles and four books. His research interests include computer-aided control system designs, rapid control prototyping, control and instrumentation, robot engineering, and embedded systems.

• • •